



# Total Control

*Advanced integrated supervisory and wind turbine control  
for optimal operation of large Wind Power Plants*

Flow Database for reference wind farms  
*part 2: wind farm simulations*

D1.04

Delivery date: 25.08.2020  
Lead beneficiary: KU Leuven  
Dissemination level: Public



This project has received funding  
from the European Union's Horizon  
2020 Research and Innovation  
Programme under grant agreement  
No. 727680

Author(s) information (alphabetical):		
Name	Organisation	Email
Søren Juhl Andersen	DTU	<a href="mailto:sjan@dtu.dk">sjan@dtu.dk</a>
Johan Meyers	KUL	<a href="mailto:Johan.meyers@kuleuven.be">Johan.meyers@kuleuven.be</a>
Ishaan Sood	KUL	<a href="mailto:Ishaan.sood@kuleuven.be">Ishaan.sood@kuleuven.be</a>
Niels Troldborg	DTU	<a href="mailto:niet@dtu.dk">niet@dtu.dk</a>

## Document information

Version	Date	Description		
		Prepared by	Reviewed by	Approved by
1	25.08.2020	Ishaan Sood	Johan Meyers	Gunner Chr. Larsen

# TABLE OF CONTENTS

1.	Executive summary .....	4
2.	Introduction .....	4
3.	TotalControl Reference Wind Power Plant.....	5
4.	Virtual Wind Farm Environment .....	5
4.1.	Governing equations.....	6
4.2.	Simulation platforms .....	6
4.2.1.	SP-Wind (KU Leuven) .....	6
4.2.2.	EllipSys-3D (DTU) .....	7
4.3.	Simulation domains and numerical setup.....	7
5.	Pressure-driven Boundary Layer Cases .....	9
5.1.	Case description.....	9
5.1.1.	Simulation parameters .....	9
5.2.	Wind farm simulation results.....	10
6.	Conventionally-neutral Atmospheric Boundary Layer Cases.....	11
6.1.	Case description.....	11
6.2.	Wind farm simulation results.....	12
6.2.1.	SP-Wind Results .....	12
6.2.2.	EllipSys3D results.....	15
7.	Access to datasets .....	17
7.1	KU Leuven DataBase.....	17
7.2	DTU DataBase .....	19
8.	REFERENCES .....	19

## 1. EXECUTIVE SUMMARY

One of the core activities within the TotalControl project is the development and validation of appropriate end-to-end wind-farm simulation models that cover the whole chain from flow model over aero-elastic model to power-grid model. Proper validation of control and design oriented engineering models requires accurate reference data. In addition to the available field measurement data, which in practice tends to be sparse and case-specific, high-fidelity Large Eddy Simulation (LES) tools provide a virtual wind farm environment from which rich numerical measurements can be taken under controlled conditions.

The current report discusses the wind farm simulation runs using previously generated precursor input data (detailed in part 1 of deliverable report). The data are generated using two independent LES codes. The simulation cases can be categorized into two groups: a set of canonical Pressure Driven Boundary Layers (PDBL) and a set of atmospheric boundary layers with neutral stratification and a capping inversion on top (so-called Conventionally Neutral Boundary Layers (CNBLs)). Subsets of the generated data have been made publically available and further data is available upon request.

## 2. INTRODUCTION

One of the core activities within the TotalControl project is the development and validation of appropriate end-to-end wind-farm simulation models that cover the whole chain from flow model over aero-elastic model to power-grid model. Proper validation of control- and design-oriented engineering models requires accurate reference data. In addition to the available field measurement data, which in practice tends to be sparse and case-specific, high-fidelity large-eddy simulation (LES) tools provide a virtual wind-farm environment, from which rich numerical measurements can be taken under controlled conditions. In this regard, a high-fidelity reference database is generated using two independent numerical platforms.

The data included in the TotalControl flow database consists of two parts. The first part (further denoted as precursor data) contains unsteady three-dimensional flow data of an unperturbed atmospheric boundary layer (i.e. without the influence of turbines). This data can be used as input for an offline aero-elastic model, or as a way of characterizing incoming atmospheric flow conditions. The second part contains data obtained from simulations including turbines. The inlet conditions of the latter simulations are derived from the precursor data itself. Data from this second part can be used to characterize and benchmark wake interaction, power extraction, and turbine loading within a wind farm. The previous deliverable document focused on the first part, i.e. the precursor data of atmospheric boundary layer simulations without any turbines and the data is publically available in the online Zenodo repository at <https://zenodo.org/communities/totalcontrolflowdatabase/>. This report is a follow up document, containing wind farm data generated using the inflow precursor data from the former report. The data for the wind farm simulations is available at <https://zenodo.org/communities/totalcontrolwindfarmdatabase/>

The specifications of the simulation cases have been designed through a series of discussions between the authors of this document. The cases can be divided into two main categories: on the one hand, canonical pressure-driven boundary layer cases are used as a simplified surrogate for a neutral atmospheric boundary layer; on the other hand, actual atmospheric boundary layers with a conventionally neutral stratification are simulated, i.e. including Coriolis and buoyancy forces. Each of these categories can further be divided in terms of turbulence intensity and wind direction.

The document is outlined as follows. First, a brief review of the considered wind farm and turbine is given. Then, the virtual environment to simulate the wind farm operation is discussed. Next, different wind farm flow cases for the PDBL and CNBL inflows are detailed, along with farm performance results. Finally, the document is concluded with a detailed description of the dataset availability and general scripts to load in the data files.

### 3. TOTALCONTROL REFERENCE WIND POWER PLANT

The TotalControl Reference Wind Power Plant (TC RWP) has been defined in deliverable D1\_03 (Andersen et al., 2018). The TC RWP consists of 32 turbines in a staggered pattern, see Figure 1. The choice of a staggered pattern is somewhat arbitrary; but it makes sense to arrange the turbines in this manner if the prevailing wind direction were from the left. The reference turbines are the DTU 10 MW turbines (Bak et al., 2013), with a hub height of 119 m and a rotor diameter of 178.3 m.

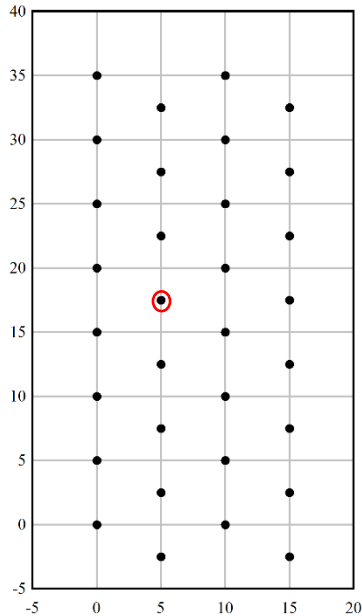


Figure 1: Layout of the TC RWP. Axes have units of  $s/D$ , with a rotor diameter  $D = 178.3$  m. Turbine 2.5 is circled in red.

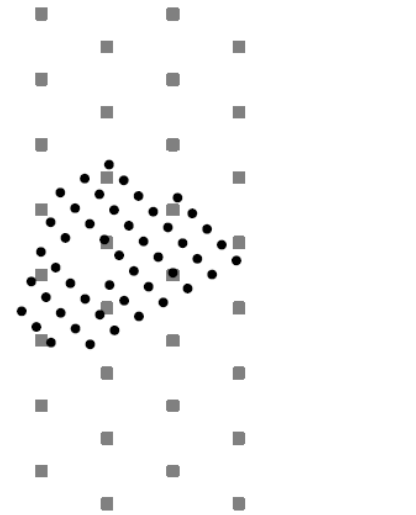


Figure 2: Scale comparison of the TC RWP (gray) and the Lillgrund WP (black)

The number of turbines results from a compromise between limiting the computational cost of high-resolution flow simulations and having an array that is large enough to be relevant as an offshore wind power plant. Figure 2 shows a scale comparison of the TC RWP to the Lillgrund plant, also featured in the TotalControl project.

The columns of eight turbines (vertical in Figure 1) provide a "long" direction where the turbine-to-turbine wake effects can approach their asymptotic values. Furthermore, given a top-down wind direction a typical aligned layout is achieved, for which wake redirection was found to be a very efficient wind-farm control strategy (Munters and Meyers 2018). In the perpendicular "short" direction (horizontal in Figure 1) only two turbines are directly aligned. For a left-right wind direction, a standard staggered configuration is achieved, for which wake induction control strategies have been found to be more suitable. In this way, both the redirection and induction approach to wind-farm control can be investigated without a priori favouring one over the other based on wind-farm layout. Different wind inflow directions can be achieved by rotating the entire wind farm by the desired inflow angle, e.g. 30 and 60 degree cases (Figure 3).

The data from the turbine highlighted in row 2 position 5 of figure 1, from here on referred as turbine 2.5, is used for visualizing aeroelastic results as well as velocity field data in subsequent sections.

### 4. VIRTUAL WIND FARM ENVIRONMENT

The virtual wind farm environment used for generating the flow database consists of two independent numerical solvers, each with their own characteristics, solving the same governing equations for atmospheric boundary-layer flow. Firstly, the governing equations are detailed, and afterwards the SP-Wind and EllipSys 3D numerical solvers are discussed.

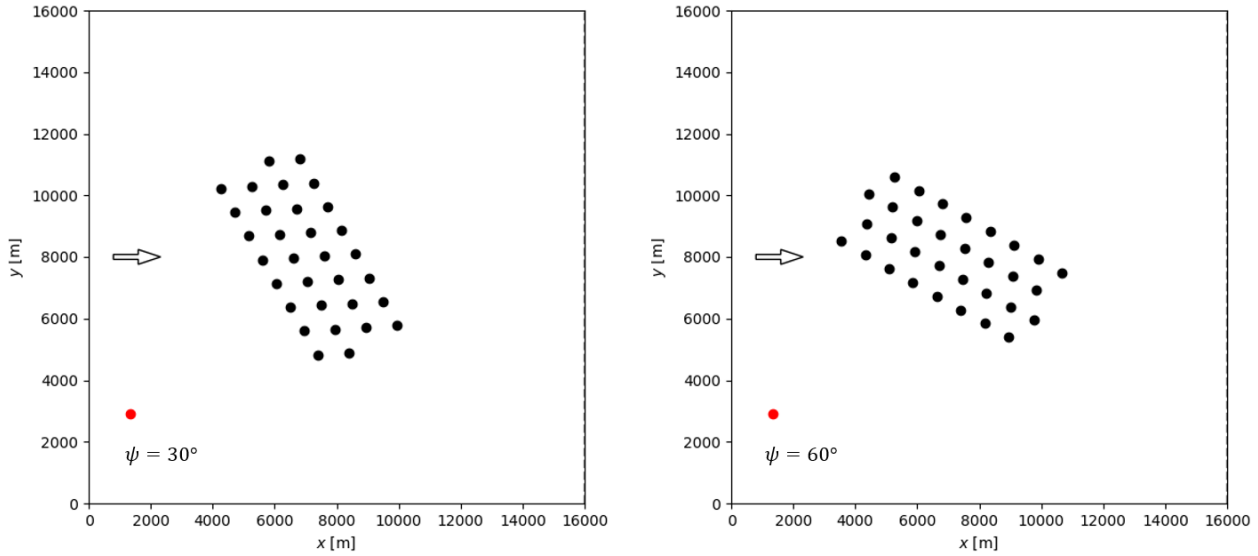


Figure 3 Reference wind farm rotated by a) 30 and b) 60 degrees to simulate different inflow wind directions

#### 4.1. GOVERNING EQUATIONS

All simulations are based on the three-dimensional, unsteady, and spatially filtered Navier-Stokes momentum and temperature equations

$$\frac{\partial \tilde{\mathbf{u}}}{\partial t} + (\tilde{\mathbf{u}} \cdot \nabla) \tilde{\mathbf{u}} = -\frac{\nabla(\tilde{p} + p_\infty)}{\rho} - \nabla \cdot \boldsymbol{\tau}_s + 2\boldsymbol{\Omega} \times \tilde{\mathbf{u}} + \mathbf{g}(\tilde{\theta} - \theta_0)/\theta_0 + \boldsymbol{\tau}_w + \mathbf{f}$$

$$\frac{\partial \tilde{\theta}}{\partial t} + (\tilde{\mathbf{u}} \cdot \nabla) \tilde{\theta} = -\nabla \cdot \mathbf{q}_s$$

which are solved by means of Large-Eddy Simulation. In these equations,  $\tilde{\mathbf{u}}$  and  $\tilde{p}$  are the filtered velocity and pressure fields respectively. Further,  $\tilde{\theta}$  is the filtered potential temperature field, and  $\theta_0$  is the background adiabatic base state. The pressure gradient is readily split into a background pressure gradient  $\nabla p_\infty$  driving the mean flow, and a fluctuating component  $\nabla \tilde{p}$ . The very high Reynolds numbers in atmospheric boundary-layer flows combined with typical spatial resolutions in LES justify the omission of resolved effects of viscous momentum transfer and diffusive heat transfer. Instead, these are represented by modeling the subgrid-scale stress tensor  $\boldsymbol{\tau}_s$  and the subgrid-scale heat flux  $\mathbf{q}_s$  originating from spatially filtering the original governing equations. Coriolis effects are included through the Earth's angular velocity vector  $\boldsymbol{\Omega}$ , and thermal buoyancy is represented by  $\mathbf{g}(\theta - \theta_0)/\theta_0$ , with  $\mathbf{g}$  the gravitational acceleration  $\tilde{\theta}$  the filtered potential temperature and  $\theta_0$  a reference temperature. The effect of the sea surface is included using a rough-wall stress boundary  $\boldsymbol{\tau}_w$ , corresponding to a logarithmic velocity profile with a roughness length  $z_0$ . Finally,  $\mathbf{f}$  represents any remaining body forces (e.g. by wind turbines) on the flow.

#### 4.2. SIMULATION PLATFORMS

Simulations are performed by KU Leuven (using SP-Wind), and by DTU (using EllipSys3D). A short description of these simulation platforms is given below.

##### 4.2.1. SP-WIND (KU LEUVEN)

SP-Wind is a wind-farm LES code built on a high-order flow solver developed over the last 10 years at KU Leuven (Calaf, Meneveau & Meyers 2010; Munters, Meneveau & Meyers 2016; Allaerts & Meyers 2017). Spatial discretization is performed by combining pseudo-spectral schemes with fourth-order energy-conservative finite differences. The equations are marched in time using a fully explicit fourth-order Runge-Kutta scheme, and grid partitioning is achieved

through a scalable pencil decomposition approach. Subgrid-scale stresses are modeled with a standard Smagorinsky model with wall damping. The subgrid-scale heat flux is calculated from the resolved potential temperature profile using an eddy-diffusivity model. The DTU 10MW turbines are modeled by an actuator sector (AS) model, coupled with a nonlinear flexible multi-body dynamics model (Vitsas and Meyers 2016). Turbines are controlled using an implementation of the DTU wind energy controller (Hansen et al. 2013), however, the feature of pitching the turbine blades at low wind speeds is not included.

Turbulent inflow conditions for wind-farm simulations are generated in separate precursor simulations (see e.g. Munters, Meneveau & Meyers 2016). A streamwise slab of the velocity and temperature field is stored to disk when running the precursor, and is later introduced in the wind-farm domain by means of body forces in a so-called fringe region.

#### 4.2.2. ELLIPSYS-3D (DTU)

EllipSys-3D is a general-purpose flow solver (Michelsen 1992, Sørensen 1994), solving the discretized incompressible Navier – Stokes equations in general curvilinear coordinates using a block-structured finite-volume approach. Pressure coupling is achieved using the SIMPLE algorithm with Rhie-Chow momentum interpolation. The convective terms are discretized using the fourth order central difference scheme. The subgrid-scale stresses are modeled with Deardorff model. The turbines are modeled using two different methods, namely the actuator disc/sector (AS) method (Mikkelsen 2004) and the actuator line method (AL) (Sørensen and Shen 2002). The former has the advantage of enabling larger time steps, while the latter provides a more detailed representation of the turbines, which particular has an impact in the near wake behind the individual turbines. Both methods have been fully coupled to the aero-elastic tool, Flex5 (Øye 1996). Turbulent inflow is also generated in separate precursor simulations, where the velocities are extracted at a given plane in the domain and saved for later use. These will be introduced directly on the inflow boundary in the simulations of wind-farms.

### 4.3. SIMULATION DOMAINS AND NUMERICAL SETUP

The simulation domain has a size of  $16 \times 16 \times 1.5 \text{ km}^3$  in the streamwise, spanwise, and vertical directions respectively (see Figure 4). This size is a compromise between having a small blockage of the turbines in the domain (in the eventual upcoming wind farm simulations) and keeping computational costs reasonable. In the simulations by KUL the grid resolution is  $13.33 \times 13.33 \times 6.66 \text{ m}^3$ , resulting in a computational grid of  $1200 \times 1200 \times 225 = 324 \times 10^6$  gridpoints. In the precursor simulations by DTU the number of grid cells are slightly less; namely  $1184 \times 1184 \times 224 = 314 \times 10^6$ . Besides the grids used by DTU the subsequent wind farm simulations utilize that EllipSys allows stretching of the grids. For these simulations the grids are kept equidistant in the regions surrounding the wind farm, while the cells are stretched towards the outer boundaries. In practice this allow reducing the number of cells significantly without compromising the grid resolution in the region of the wind farm. For example, the mesh used for the simulations where the wind comes from 90 degrees only uses  $896 \times 576 \times 224 = 99 \times 10^6$  cells. Furthermore, the figure shows a typical precursor flow field at hub height, indicating that the domain size is large enough to encompass several instances of the large streamwise-elongated structures in the turbulent flow.

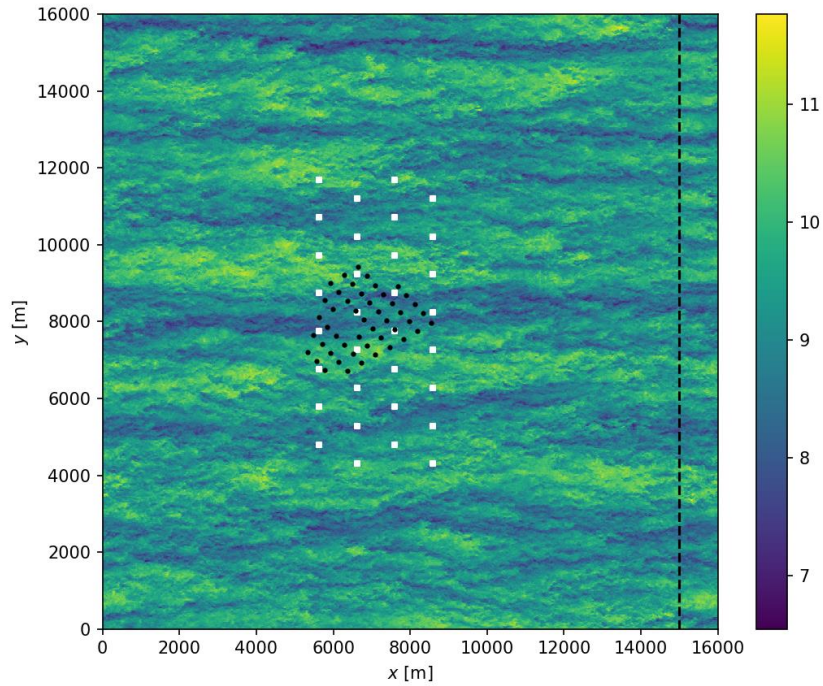


Figure 4: Planview of Lillgrund (black) and TotalControl Reference wind farm layout (white) in simulation domain. The black dashed line indicates the extent of the slab from which inflow data is extracted from the precursor simulation (without turbines). The background is colored with a typical instantaneous streamwise velocity field at turbine hub height in a precursor simulation without turbines.

Wind-farm simulations are performed in a sequence of steps. Firstly, a fully-developed turbulent boundary layer is generated in a so-called *spinup* simulation with periodic boundary conditions but without turbines. Further details of the spinup simulations to generate the precursor data can be found in the former report (Andersen et al., 2019). The data from the precursor simulations can be fed as inflow conditions to a set of wind-farm configurations. The flow is allowed to pass through the wind farm for 15 minutes to account for start-up transients, after which data collection and computation of flow statistics is done. The wind farm simulations are run for a time period of 60 minutes. The SP-Wind simulations has a LES time step of 0.5 second, while the EllipSys3D time step is 0.5 second for the actuator disc simulations and 0.025 seconds for the actuator line simulations.

The aero-elastic computations are generally performed with a much smaller time step than the flow simulations. The multi-body structural solver in SP-Wind uses a time step of 0.01 seconds, while the Flex5 computations running in EllipSys3D has a time step of 0.02 seconds.

The general domain and time parameters discussed in the current and previous paragraph are summarized in Table 1.

Table 1: General domain parameters

Domain size	$L_x \times L_y \times L_z$	$16 \times 16 \times 1.5 \text{ km}^3$
Grid	$N_x \times N_y \times N_z$	$1200 \times 1200 \times 225$
Resolution	$\Delta_x \times \Delta_y \times \Delta_z$	$13.33 \times 13.33 \times 6.66 \text{ m}^3$
Wind farm spinup time	$T_{spin}$	$15min$
Simulation time	$T$	$60min$
LES Time step	$\Delta t_{LES}$	0.5/0.025 s (AS/AL simulations)
Structural time step	$\Delta t_{struct}$	0.01/0.02 s (KUL multi-body/Flex5)

## 5. PRESSURE-DRIVEN BOUNDARY LAYER CASES

Fully-developed canonical pressure-driven boundary layers (PDBLs, alternatively half-channel flows in literature) at high Reynolds numbers have since long been used as simplified surrogates for an actual atmospheric boundary layer flow (see, e.g., Ivanell et al. (2007); Calaf et al. (2010)). The governing equations are simplified from the ABL equations shown above by omitting the equation for temperature  $\theta$  as well as any terms related to Coriolis forces and thermal buoyancy, resulting in

$$\frac{\partial \tilde{\mathbf{u}}}{\partial t} + (\tilde{\mathbf{u}} \cdot \nabla) \tilde{\mathbf{u}} = -\nabla(\tilde{p} + p_\infty)/\rho - \nabla \cdot \boldsymbol{\tau}_s + \mathbf{f}$$

### 5.1. CASE DESCRIPTION

The KUL spinups are initialized with a mean logarithmic velocity profile, upon which random divergence-free perturbations are added. These initial conditions are then advanced in time for 20 physical hours, after which the influence of the unphysical perturbations has disappeared, and the flow has reached a fully turbulent and statistically stationary state. The DTU spinups are initialized with the same mean profiles but without adding random perturbations. Furthermore, the DTU spinups are only advanced in time for about 15 hours, which unfortunately turned out was not enough to reach a fully statistically steady state. Thus, these spinups essentially includes a temporal development of the horizontal averaged conditions.

#### 5.1.1. SIMULATION PARAMETERS

The rough-wall turbulent boundary layer has a mean-flow profile  $U(z)$  following the log-law

$$U(z) = \frac{u_*}{\kappa} \ln \frac{z}{z_0}$$

with  $\kappa$  the von Kármán constant and  $u_* = \sqrt{-H/\rho \nabla p_\infty}$  the friction velocity. Simulations are performed for a typical friction velocity in offshore boundary layers of  $u_* = 0.28$  m/s, which requires a driving pressure gradient  $\nabla p_\infty/\rho = -5.2267 \times 10^{-5}$  m/s<sup>2</sup>. The dataset contains a base case with a standard offshore roughness length of  $2 \times 10^{-4}$  m, performed by both SP-Wind and EllipSys3D. Furthermore, another cases with a higher roughness length  $z_0$  of  $2 \times 10^{-3}$  m, is performed, resulting in a different turbulence intensity at turbine height.

Table 2: PDBL cases

Simulation parameters				
	Friction velocity	$u_*$		0.28 m/s
	Driving pressure gradient	$\nabla(p_\infty)/\rho$		$-5.2267 \times 10^{-5}$ m/s <sup>2</sup>
Inflows				
	PDK	KU Leuven		$z_0 = 2 \times 10^{-4}$ m
	PDKhi	KU Leuven		$z_0 = 2 \times 10^{-3}$ m
Simulation cases				
	PDKhi 0	KU Leuven	$\psi = 0^\circ$	$V_\infty = 7.8$ m/s (h = 119m)
	PDK 0	KU Leuven	$\psi = 0^\circ$	$V_\infty = 9.4$ m/s (h = 119m)
	PDK 30	KU Leuven	$\psi = 30^\circ$	$V_\infty = 9.4$ m/s (h = 119m)
	PDK 90	KU Leuven	$\psi = 90^\circ$	$V_\infty = 9.4$ m/s (h = 119m)

### 5.2. WIND FARM SIMULATION RESULTS

Detailed description of the KU Leuven PDBL precursor simulations have already been presented in the D 1.04 part 1 report, available at : <https://cordis.europa.eu/project/id/727680/results>. Figure 5 b) below shows average row power for the PDBL cases, averaged across each row (comprising of 8 turbines) and over time. The average power in the PDK cases is higher than in the PDKhi case, due to greater mean hub height velocity of the precursor inflow. Both the 0° farm configuration cases have sharp dip in average power in rows 3 and 4, as the turbines in these rows are operating in the wakes of those in rows 1 and 2 respectively. A power spike can be observed in row 3 of the 30° farm configuration as the top most turbine in this row is operating in un-waked conditions (evident in figure 3a), therefore boosting average row power. The 90° aligned wind inflow case has the lowest average row power due to 7 turbines in each row operating in fully waked conditions.

Comparing the flapwise blade root bending moments in the turbine 2.5 (figure 6), higher moments can be observed in the PDK 0 case compared to PDKhi 0 case due to higher thrust generation. The PDK 90 case has moments of lower magnitude due to the turbine operating in a waked condition in the fully aligned configuration. However, the larger variation in moments results in larger structural fatigue, as presented in the next section.

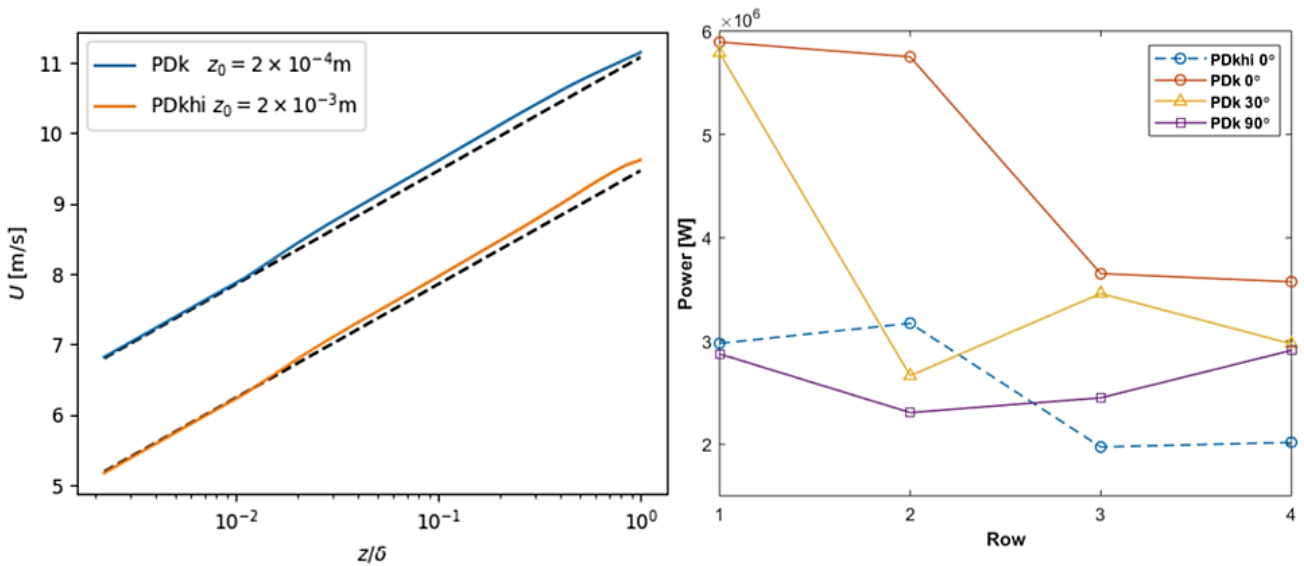


Figure 5 a) Flow profiles for PDBL cases b) Average row power for different PDBL inflow cases. Rows are numbered left to right in the staggered representation of figure 1

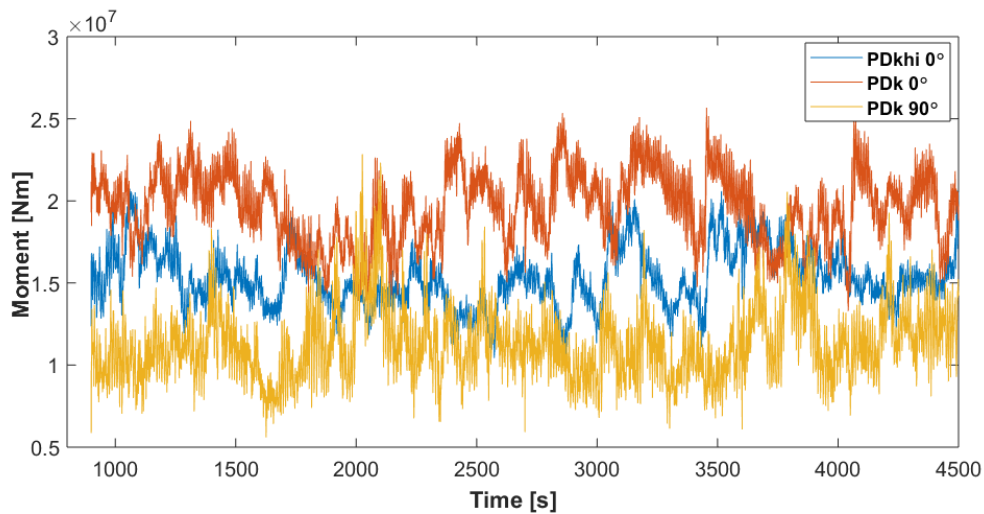


Figure 6 Flapwise blade root bending moments of the turbine 2.5, highlighted in figure 1)

## 6. CONVENTIONALLY-NEUTRAL ATMOSPHERIC BOUNDARY LAYER CASES

The current section discusses the definition and results of the conventionally neutral atmospheric boundary layer cases (CNBLs). The conventionally neutral boundary layer consists of a neutral boundary layer, capped by a strongly stable inversion layer. Above the CNBL, the free atmosphere is stably stratified with a constant potential temperature gradient. Such a boundary layer can form, for instance, with wind blowing from onshore to the sea in daytime during spring (when the sea surface temperature is still relatively cold). The change in surface roughness and heat flux will cause a growing stable internal boundary layer, which eventually results in a neutral boundary layer capped by a stable inversion layer.

### 6.1. CASE DESCRIPTION

The simulation cases included in the current dataset are designed based on similar precursor cases for wind-farm LES discussed in Allaerts & Meyers (2017). Cases are forced with a constant geostrophic wind speed of  $G = 12 \text{ m/s}$  and the base wall roughness length is  $z_0 = 2 \times 10^{-4} \text{ m}$ . The lapse rate in the stably-stratified free atmosphere is  $\gamma = 1 \text{ K/km}$ , and the temperature of the mixed layer is  $\theta_m = 15^\circ$ , which is also taken as the reference temperature. The Coriolis parameter is  $f_c = 10^{-4} \text{ s}^{-1}$ , corresponding to a latitude of  $43.43^\circ$ .

In contrast to the PDBL cases where the boundary layer grows naturally to the top of the domain, in the CNBL cases, the height of the boundary layer will result from a balance between entrainment on the one hand and a stably stratified free atmosphere and capping inversion on the other. An empirical formula for this height  $h$  is given by

$$h = A \frac{\theta_0}{g \Delta \theta} u_*^2,$$

with  $A \approx 500$  an empirical parameter and  $\Delta \theta$  the strength of the capping inversion.

KU Leuven simulations focus on varying the boundary layer height by choosing different capping inversion strengths ( $\Delta \theta = 2\text{K}, 4\text{K}, 8\text{K}$  with equilibrium boundary layers at  $500\text{m}, 250\text{m}$  and  $125\text{m}$  respectively). DTU simulations focus on different inflow turbulence intensities by varying the wall roughness. Simulation parameters and cases are summarized in Table 3. Further details regarding the setup and results of the CNBL precursor simulations have already been presented in the D 1.04 part 1 report.

Table 3: CNBL cases

Simulation parameters				
	Geostrophic wind	$G$		$12 \text{ m/s}$
	Coriolis parameter	$f_c$		$10^{-4} \text{ s}^{-1}$
Inflows				
	CNk2	KU Leuven	$z_0 = 2 \times 10^{-4} \text{ m}$	$\Delta \theta = 2\text{K} (h = 500\text{m})$
	CNk4	KU Leuven	$z_0 = 2 \times 10^{-4} \text{ m}$	$\Delta \theta = 4\text{K} (h = 250\text{m})$
	CNk8	KU Leuven	$z_0 = 2 \times 10^{-4} \text{ m}$	$\Delta \theta = 8\text{K} (h = 125\text{m})$
	CNz24	DTU	$z_0 = 2 \times 10^{-4} \text{ m}$	$\Delta \theta = 2\text{K} (h = 500\text{m})$
	CNz23	DTU	$z_0 = 2 \times 10^{-3} \text{ m}$	$\Delta \theta = 2\text{K} (h = 500\text{m})$
	CNz25	DTU	$z_0 = 2 \times 10^{-5} \text{ m}$	$\Delta \theta = 2\text{K} (h = 500\text{m})$

**Simulation cases**

CNk2 30	KU Leuven	$\psi = 30^\circ$	$V_\infty = 11 \text{ m/s}$ (h = 119m)
CNk2 60	KU Leuven	$\psi = 60^\circ$	$V_\infty = 11 \text{ m/s}$ (h = 119m)
CNk4 30	KU Leuven	$\psi = 30^\circ$	$V_\infty = 11.3 \text{ m/s}$ (h = 119m)
CNk4 90	KU Leuven	$\psi = 90^\circ$	$V_\infty = 11.3 \text{ m/s}$ (h = 119m)
CNk8 0	KU Leuven	$\psi = 0^\circ$	$V_\infty = 11.4 \text{ m/s}$ (h = 119m)
CNk8 90	KU Leuven	$\psi = 90^\circ$	$V_\infty = 11.4 \text{ m/s}$ (h = 119m)
CNz23 00	DTU	$\psi = 0^\circ$	$V_\infty = 10.5 \text{ m/s}$ (h=119m)
CNz23 90	DTU	$\psi = 90^\circ$	$V_\infty = 10.5 \text{ m/s}$ (h = 119m)
CNz24 00	DTU	$\psi = 0^\circ$	$V_\infty = 11 \text{ m/s}$ (h = 119m)
CNz24 30	DTU	$\psi = 30^\circ$	$V_\infty = 11 \text{ m/s}$ (h = 119m)
CNz24 45	DTU	$\psi = 45^\circ$	$V_\infty = 11 \text{ m/s}$ (h = 119m)
CNz24 60	DTU	$\psi = 60^\circ$	$V_\infty = 11 \text{ m/s}$ (h = 119m)
CNz24 90	DTU	$\psi = 90^\circ$	$V_\infty = 11 \text{ m/s}$ (h = 119m)
CNz25 00	DTU	$\psi = 0^\circ$	$V_\infty = 11.6 \text{ m/s}$ (h = 119m)
CNz25 90	DTU	$\psi = 90^\circ$	$V_\infty = 11.6 \text{ m/s}$ (h = 119m)

## 6.2. WIND FARM SIMULATION RESULTS

### 6.2.1. SP-WIND RESULTS

The initial conditions for the mean wind velocity vector along the domain height as well as the temperature are shown for the CNk2, CNk4 and CNk8 cases in figure 7. The figure shows the smooth transition between the velocities and temperatures in the boundary layer (characterized by veered and sheared velocities with well-mixed temperature) and in the free atmosphere above the capping inversion (with uniform velocities and stable free-atmosphere stratification).

The average row power is presented in figure 8 a. Similar to the PDBL cases, a spike in power can be observed in the  $30^\circ$  configuration. The  $60^\circ$  wind inflow case has highest average row power in rows 3 and 4, due to 2 and 1 turbines operating in un-waked conditions at the top of each row respectively. Conversely, the  $90^\circ$  cases have the lowest row average power due to aligned configuration (figure 9 a). As a result, the CNk2 60 case has the highest farm power output of all the simulated cases (figure 8 b).

A wake deficit analysis was conducted to study the effect of the inflow case on wake mixing and recovery. Figure 9b) shows the vertical wake profiles behind the bottom left turbine of the farm configuration shown in figure 9a) for the fully aligned cases PDK 90, CNk4 90 and CNk8 90. While the precursor field mean inflow velocities at hub height for the CNk4 and CNk8 are of similar magnitude, the wake recovery of CNk4 is better, evident from the higher normalized velocity available at the  $x/D = 4.5$  section, which serves as the inflow to the next turbine at position  $x/D = 5$ . This can be attributed to the low boundary layer height (125 m) in the CNk8 field, causing trapped oscillatory wakes to form behind the turbines, which are avoided in the higher boundary layer height (250 m) of the CNk4 field. As a result, higher energy in the flow is available for extraction by the waked turbines in the CNk4 cases, which leads to a marginally larger overall wind farm power production (shown in figure 8b).

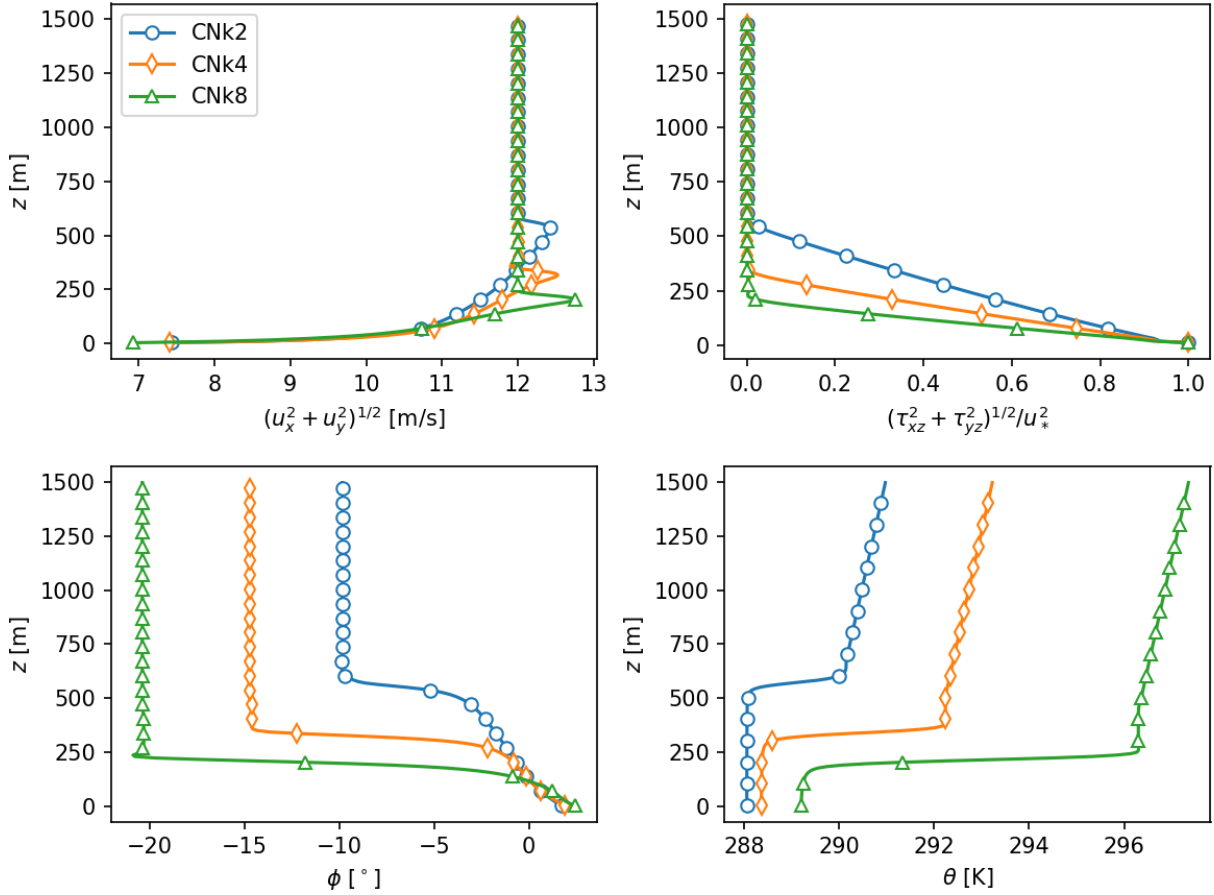


Figure 7 Flow profiles for KU Leuven CNBL cases with varying boundary layer heights. Top left: Horizontal Velocity. Top right: Total (Resolved + Subgrid) shear stress. Bottom left: Wind veer. Bottom right: Potential temperature

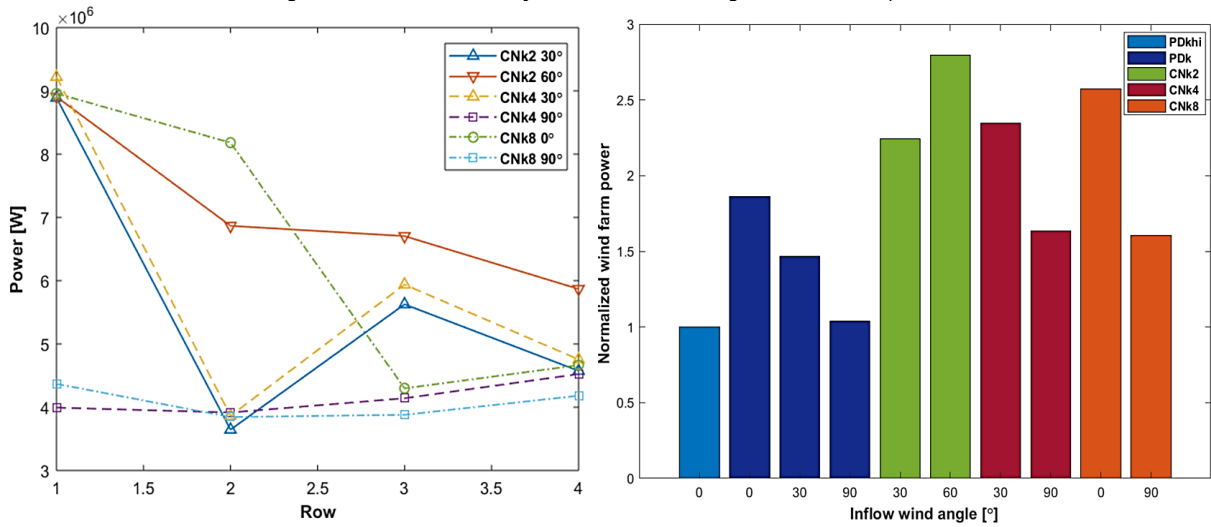


Figure 8 a) Average row power for different CNBL inflow cases. Rows are numbered left to right in the staggered representation of figure 1 b) Total wind farm power output, normalized by PDkhi 0 case

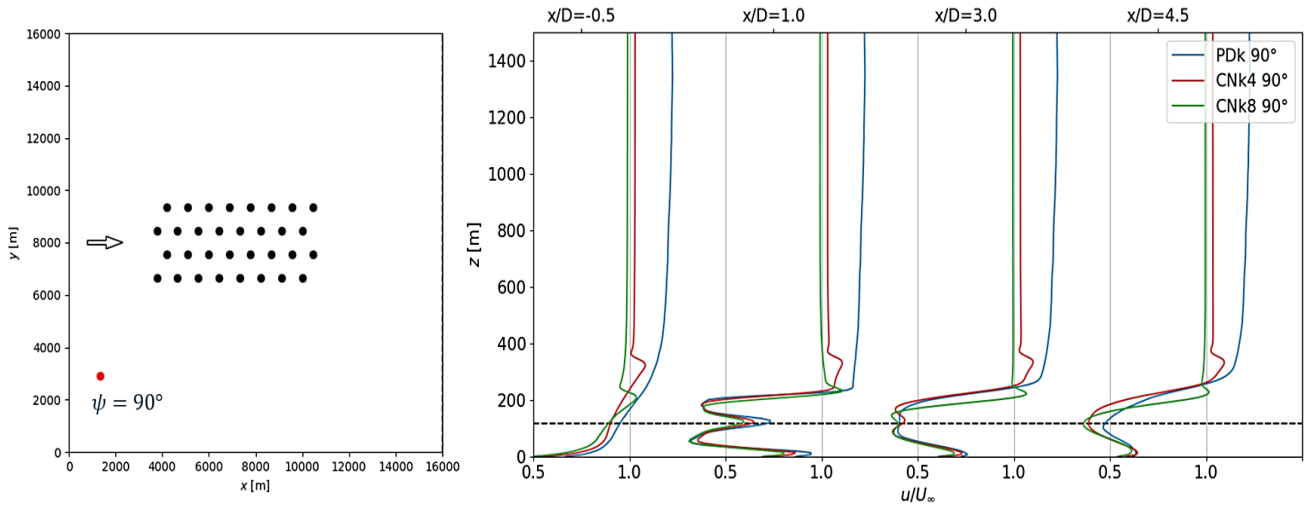


Figure 9 a) Fully aligned farm configuration for 90° inflow direction cases, b) Time averaged wake deficit for the bottom left turbine of figure a), normalized by mean free stream inflow velocity from precursor simulations. Horizontal dashed line signifies hub height (119 m)

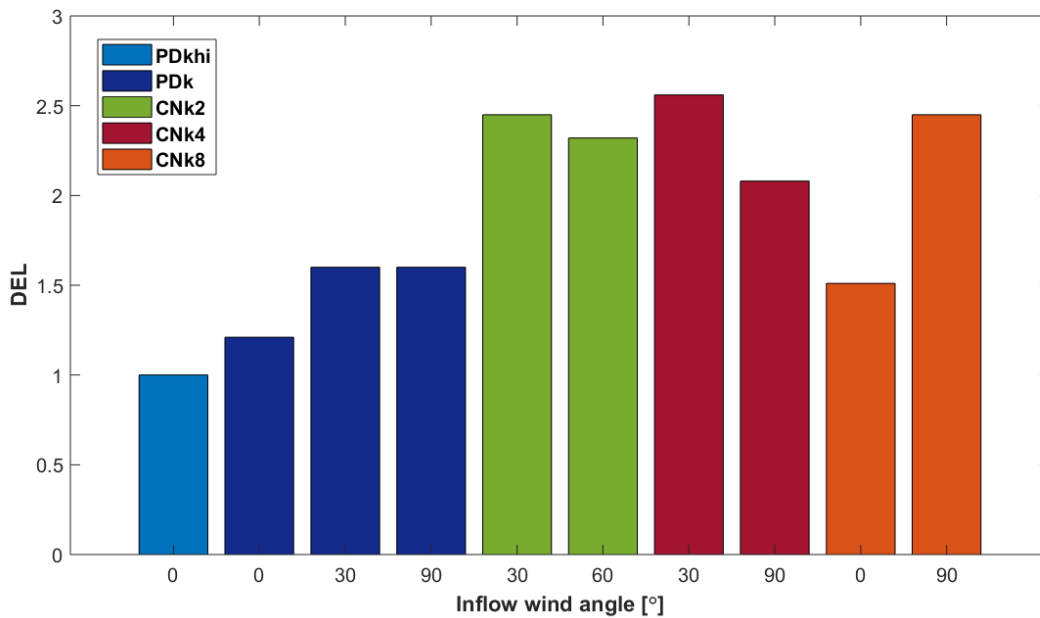


Figure 10 Flapwise blade root bending moment DEL for turbine 2.5, normalized by PDKhi 0 case

To determine the effect of fatigue, we use the damage equivalent loads (DELs) to compare the load histories of the same turbine across different cases. DEL is computed using the Palmgren-Miner rule and the Wöhler equation to account for accumulating fatigue damage caused to the wind turbine components by the fluctuating structural loads (Sutherland, 1999). The loads time series are counted and binned into individual cycles using the rainflow-counting algorithm (Downing and Socie, 1982), and for the wind turbine blades the components follow the Wöhler's curve with a slope coefficient equal to 10 (Freebury and Musial, 2000). The results of the DEL analysis for flapwise blade root bending moments for turbine 2.5 have been plotted in figure 9, and as expected, DEL for the cases in which turbine 2.5 is operating in waked conditions is significantly higher than the ones in which the turbine is facing un-waked free stream velocity. It must be noted that the omission of the pitching feature in the DTU 10MW turbine at low wind speeds may impact the fatigue damage in the waked turbines, particularly in the PDK cases with low hub height velocities, which result in wake wind speeds that fall within this operation regime. In these cases, the DEL reported in Figure 10 for the orientations in which turbine 2.5 is waked would be lower if pitching action was included.

6.2.2 ELLIPSYS3D RESULTS

The horizontal averaged conditions for the inflow for the DTU simulations are shown in Figure 11. The behavior is the same as shown in Figure 7, and we see the expected behavior with increasing boundary layer height, shear and veer with increasing roughness. It should be emphasized that the shown profiles are not fully converged, and hence they do change during the 75 minutes.

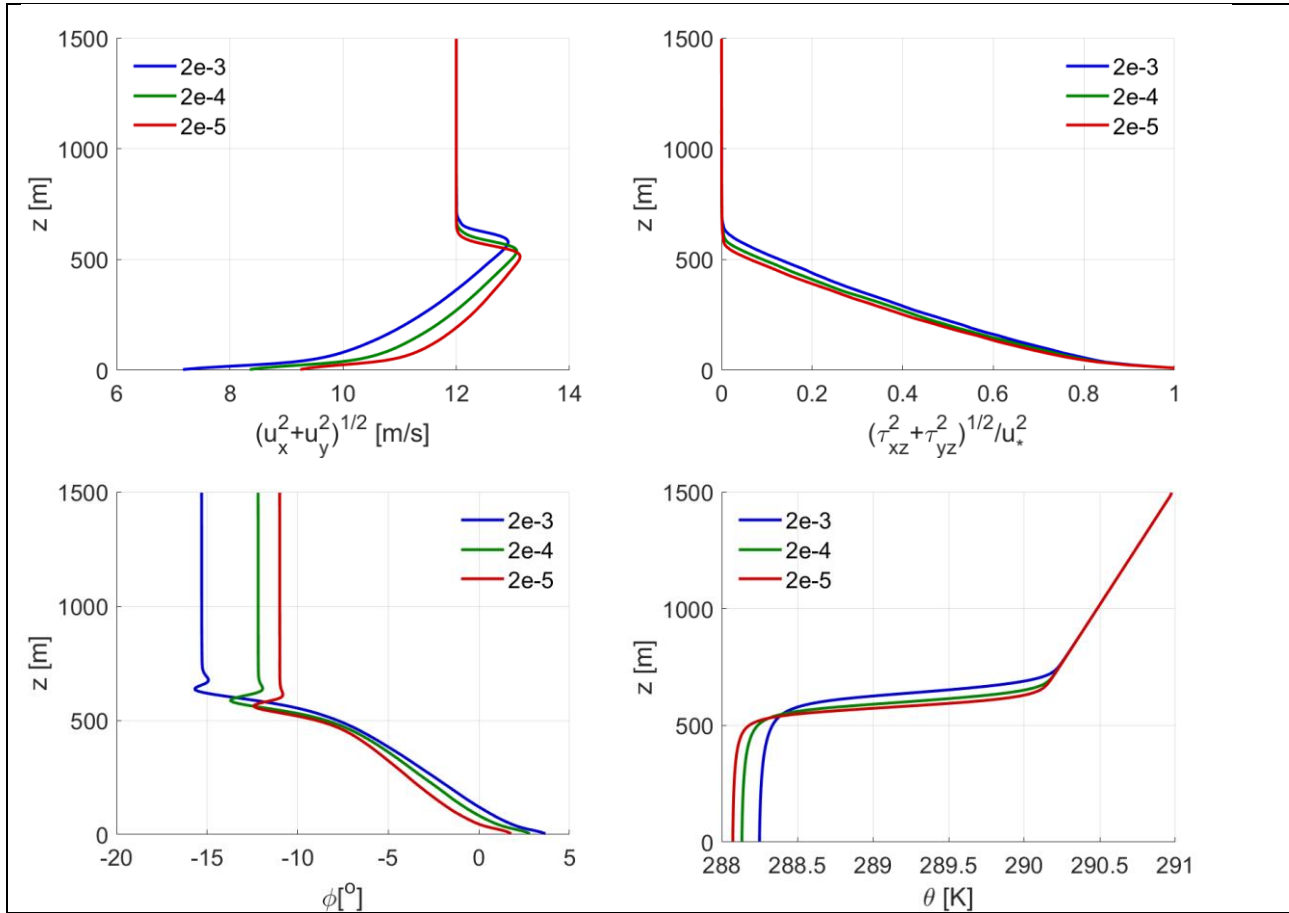


Figure 11: Initial conditions for the DTU simulations at different roughness levels

The average power production for each row is plotted in Figure 12 for the three different roughness cases. Results are shown for both the actuator disc (dark shades, broken lines) and actuator line (light shades, full line) simulations. Clearly, the tendencies are similar for the same flow cases (Figure 12a), but the power production is higher for the actuator line simulations. This is not unexpected because at this low grid resolution the choice of force smearing has a large effect on the induced velocity in the rotor plane (Mikkelsen 2004). However, for some cases the difference in power extraction also affect the wake recovery and hence trends, e.g. comparing the power production for inflow direction of 30° and  $z_0 = 2e-4$  m in Figure 12b. The actuator disc trends are comparable to those presented in Figure 8 although the power production is significantly higher due to the higher velocity in the precursor simulations.

Figure 13 shows the total wind farm power production for the different CNBL cases run using EllipSys3D, where the data has been normalized by the result from  $z_0 = 2e-4$  m. Again, results are shown for both actuator disc and actuator line. Despite having difference in the power production between actuator disc and actuator lines (Figure 12), the normalized results are almost identical. The overall wake effects are clear as the wind farm orientation change from 0° to 90°, and the power production is essentially halved for the smaller roughness cases. The high roughness of  $z_0 = 2e-5$  m yields higher turbulence and the highest overall production as there is increased wake recovery and less wake losses.

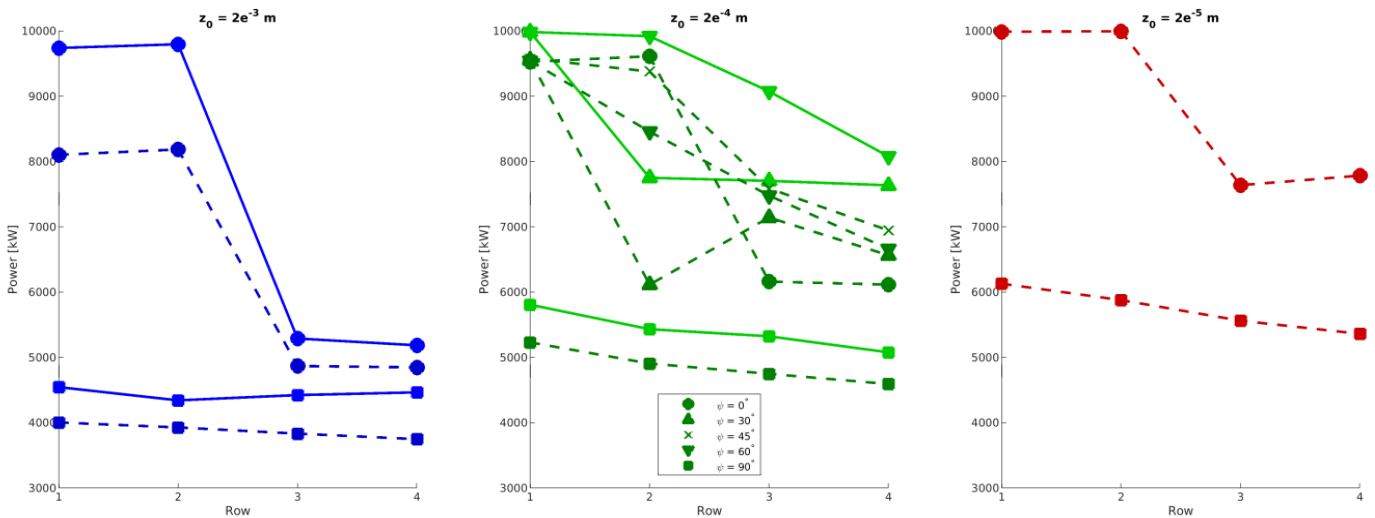


Figure 12 Average row power for different CNBL inflow cases from EllipSys3D. a)  $z_0 = 2e^{-3} m$ , b)  $z_0 = 2e^{-4} m$ , and c)  $z_0 = 2e^{-5} m$ . Darker shades and broken lines corresponds to AD simulations, while lighter shades and full lines corresponds to AL simulations.

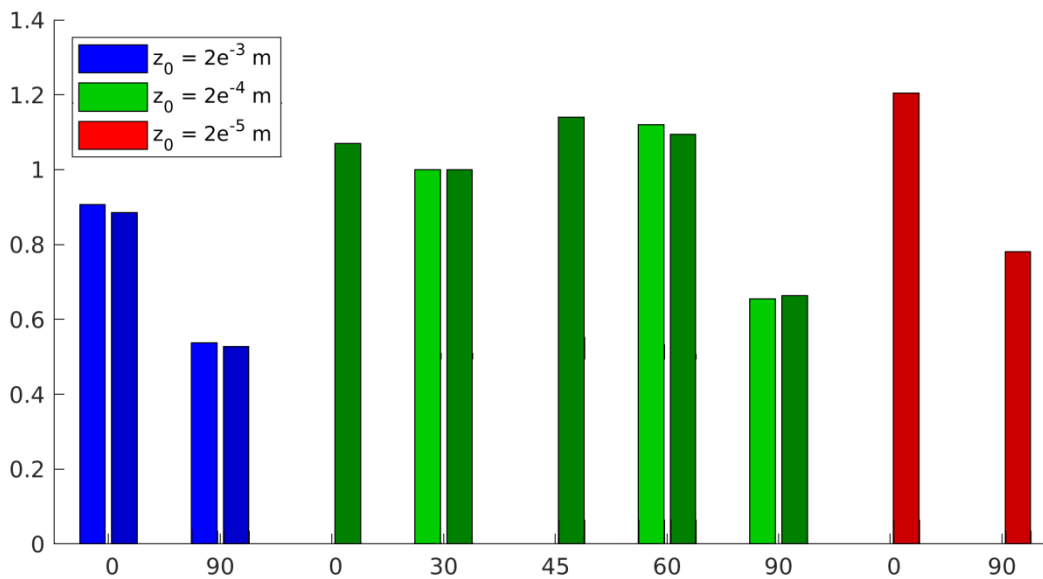


Figure 13 Total wind farm power for different CNBL inflow cases from EllipSys3D. Data has been normalized by total power for  $z_0 = 2e^{-4} m$  and 30 deg. orientation. Darker shades corresponds to AD simulations, while lighter shades corresponds to AL simulations.

Figure 14 shows mean blade pitch, mean rotational speed and median of various 10min 1Hz DEL for the flapwise bending moment. All have been normalized by  $z_0 = 2e^{-4} m$ . The DEL decreases on turbine 2.5 when the wind farm orientation changes from  $0^\circ$  to  $90^\circ$  (Figure 14C), which is surprising as the turbine is operating in wake. However, as seen the rotational speed also decreases (Figure 14a) and the pitching increases (Figure 14b), which indicates that the operational region of the turbine change. The DTU10MW starts pitching for small wind speeds, and here it results in reduction of the DEL.

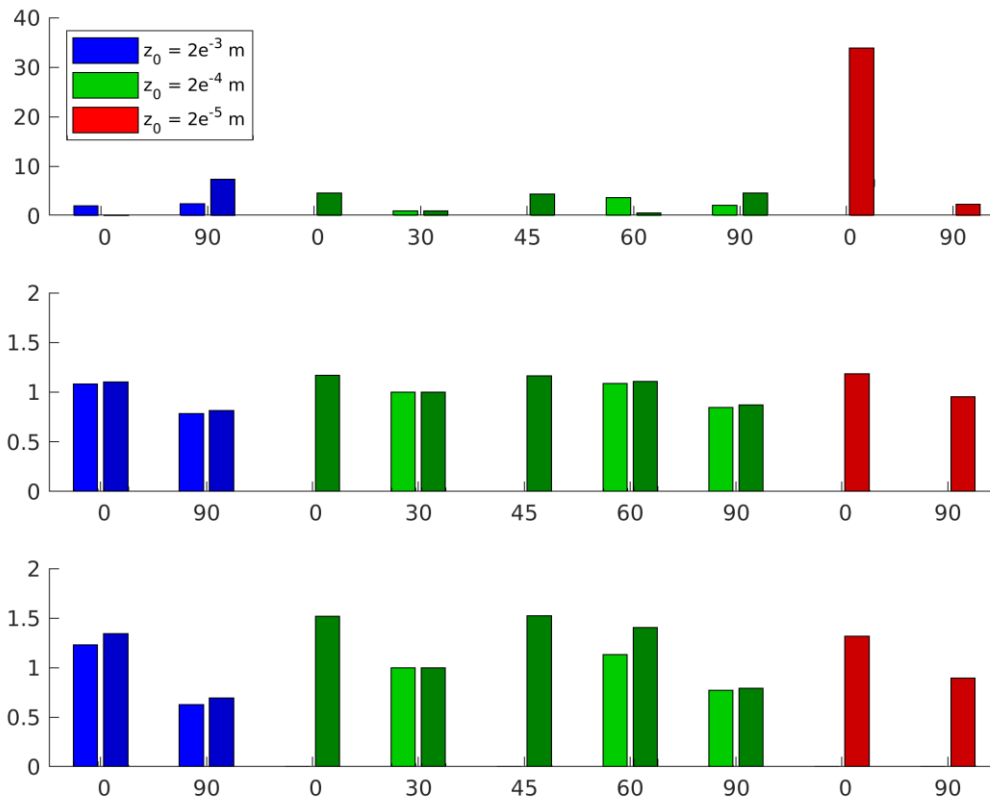


Figure 14 Operational data for turbine 2.5 for various CNBL inflow cases from EllipSys3D. a) Mean blade pitch, b) mean rotational speed, and c) median of 1 Hz 10 min DEL for flapwise bending moment. DEL has been normalized with values from  $z_0 = 2e^{-4}$  m and 30 deg. orientation. Darker shades corresponds to AD simulations, while lighter shades corresponds to AL simulations.

## 7. ACCESS TO DATASETS

### 7.1 KU LEUVEN DATABASE

The full data from the KU Leuven precursor and wind farm simulations is stored on an archiving system of the Flemish Supercomputer Center at KU Leuven. The entire dataset consists of a set of time-averaged flow variables, snapshots of the flow field ( $xy$ ,  $yz$  and  $xz$  cross sections), full turbine performance data (including aeroelastic data) and detailed flow field in a box around turbine 2.5.

A subset of this dataset is publically available in the form HDF5 files hosted on a community of Zenodo repositories at: [https://zenodo.org/communities/totalcontrolwind\\_farmdatabase/](https://zenodo.org/communities/totalcontrolwind_farmdatabase/). Additional data can be made available upon request. Information regarding the precursor simulations datasets has already been presented in the part 1 deliverable (Andersen et al., 2019). The wind farm data is split up into four files (`field_snapshot.h5`, `turb_performance.h5`, `cross_sections_timeseries.h5` and `3D_box_timeseries.h5`) in order to keep the size of each file relatively small. More specifically, the dataset consists of:

#### Snapshots: `field_snapshot.h5`, ~5GB

- A snapshot of the full velocity (+ temperature) field at  $t = 75$  min

#### Turbine performance: `turb_performance.h5`, ~5MB

- Aerodynamic performance data for all turbines at 1 Hz resolution
- Aeroelastic data for all turbines at 100 Hz resolution

**Time series: cross\_sections\_timeseries.h5, ~5GB**

- Cross section ( $xy$ ) of velocity components (+temperature) at  $z = 119$  m at 0.1 Hz resolution
- Cross section ( $xz$ ) of velocity components (+temperature) at top row of turbines at 0.1 Hz resolution

**Time series: 3D\_box\_timeseries.h5, ~5GB**

- Velocity data in a 3D box of size  $[880 \times 346.6 \times 590m^3]$  around turbine 2.5 at 1 Hz resolution for the last 15 mins of the simulation

The data repository contains different Python scripts like `plot_3D_box.py` and `plot_field.py` which can be used to import, manipulate and visualize the data. Example visualizations are shown in figures 11 and 12.

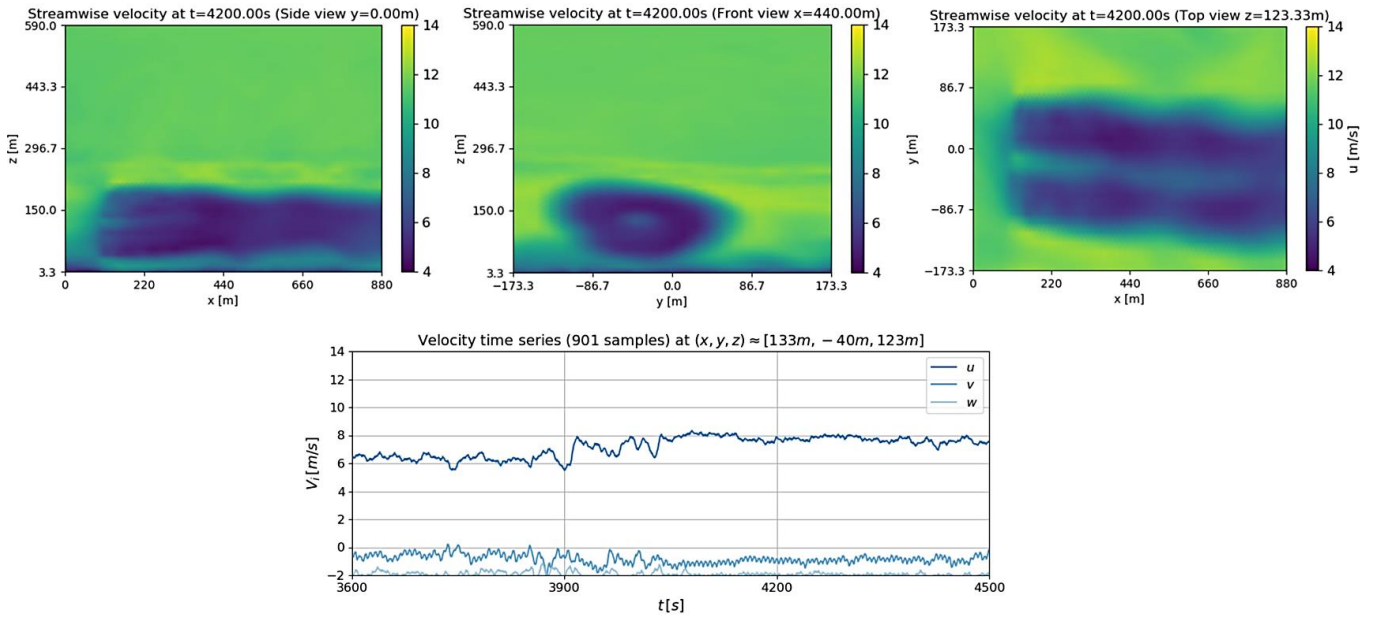


Figure 15 Top figures: Sectional views of Turbine 2.5. Bottom Figure: Time series of velocity components at a point in the 3D Box. All figures are for the CNk8 0 case

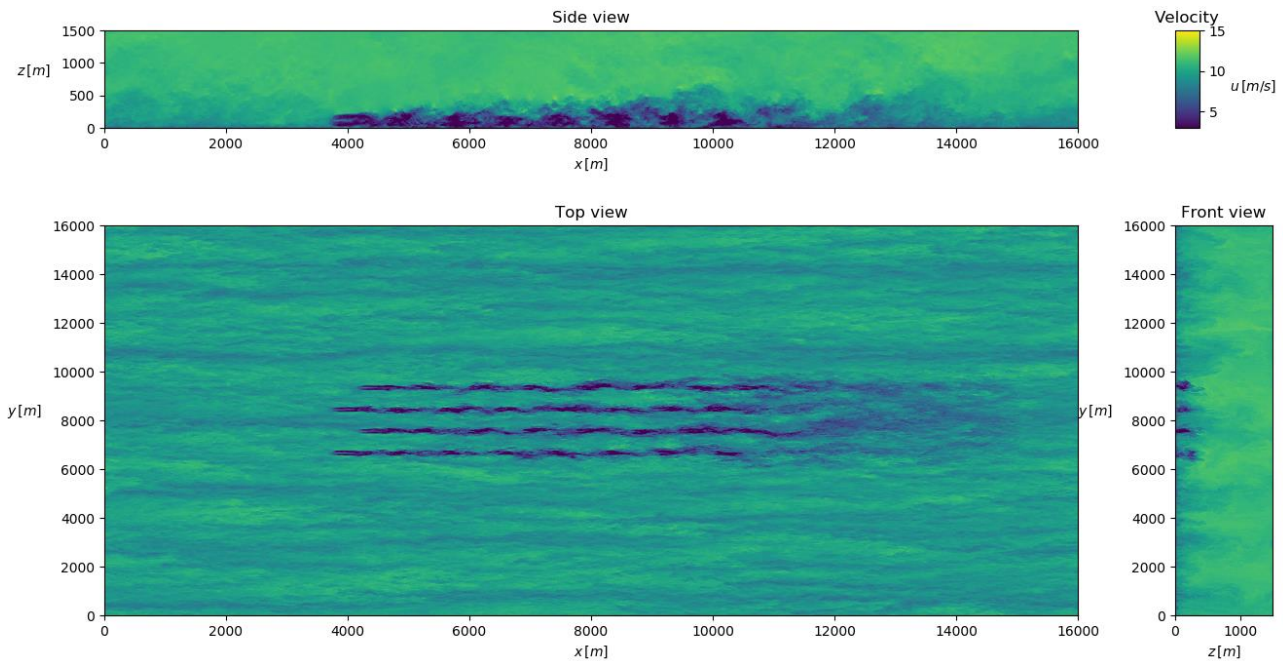


Figure 16 Top, side and front view of the instantaneous velocity field at  $t = 75$  mins for the PDK 90 case

## 7.2 DTU DATABASE

The full database from the DTU precursors and wind farm simulations is stored on the Sophia cluster at DTU. The entire dataset consists of a set of snapshots of the inflow field (xy and yz cross sections) and full turbine performance data (including aeroelastic data). A subset of the data set is publicly available in NetCDF format hosted at:

<https://data.dtu.dk/account/home#/projects/83642>

The dataset are organized in separate folder for each flow scenario and wind farm orientation. The files are given the corresponding naming where "TCal" corresponds to actuator line simulations, while "TCad" corresponds to actuator disc simulations. The dataset contains the following three datatypes with example names:

1. Horizontal (xy) planes of flow fields (u, v, and w) extracted at hub height.  
Naming: TCal\_horiz.nc
2. Vertical inflow (yz) planes of flow field (u, v, and w) extracted 1R upstream each of the 32 wind turbine (wt), which can be used as input to aero-elastic simulations.  
Naming: TCal\_inflow\_wt01.nc
3. Time series of each of the 32 wind turbines and their performance and loads. The files contain time, u velocity at hub height, power, flapwise bending moments for blade 1-3, tower bottom bending moments, thrust force, blade pitch, and rotational speed.  
Naming: TCal\_wt01.dat

Additional data can be made available upon request. Information regarding the precursor simulations datasets has already been presented in the part 1 deliverable.

## 8. REFERENCES

- Allaert D. & Meyers J. (2015). Large eddy simulation of a large wind-turbine array in a conventionally neutral atmospheric boundary layer. *Physics of Fluids* **27**, 065108.
- Allaerts D. & Meyers J. (2017). Boundary-layer development and gravity waves in conventionally neutral wind farms. *Journal of Fluid Mechanics* **814**, 95 – 130.
- Andersen, S. J., Madariaga, A., Merz, K., Meyers, J., Munters, W., & Rodriguez, C. (2018). Reference Wind Power Plant D1.03. DTU Technical Report.  
Online available at: [http://orbit.dtu.dk/files/164663085/TotalControl\\_D1\\_03\\_Reference\\_Wind\\_Farm.pdf](http://orbit.dtu.dk/files/164663085/TotalControl_D1_03_Reference_Wind_Farm.pdf)
- Andersen, S. J., Meyers, J., Munters, W., Sood, I., & Troldborg, N. (2019). Flow Database for reference wind farms part 1: precursor simulations  
Online available at:  
<https://ec.europa.eu/research/participants/documents/downloadPublic?documentIds=080166e5c3c33fee&apId=PPGMS>
- Bak C. et al. (2013). The DTU 10-MW Reference Wind turbine. DTU Technical Report.  
Online available at: <http://dtu-10mw-rwt.vindenergi.dtu.dk/>
- Calaf M., Meneveau C. & Meyers J. (2010). Large eddy simulation study of fully developed wind-turbine array boundary layers. *Physics of Fluids* **22**, 015110.
- Castro I. P. (2007). Rough-wall boundary layers: mean flow universality. *Journal of Fluid Mechanics* **585**, 469 – 485.
- G. Freebury and W. Musial. Determining equivalent damage loading for full-scale wind turbine blade fatigue tests. Proceedings of the AIAA Aerospace Sciences Meetings, Reno, NV, USA, 2000.
- H.J. Sutherland. Fatigue analysis of wind turbines. Technical report, Sandia National Laboratories, 1999.
- Ivanell S., Sørensen J.N. & Henningson D. (2007). Numerical computations of wind turbines wakes. Berlin: Springer.

- Jimenez J. (2004). Turbulent Flows over Rough Walls. *Annual Review of Fluid Mechanics* 36: 173 – 96.
- Michelsen, J. A.: Basis3D - a platform for development of multiblock PDE solvers., Tech. Rep. AFM 92-05, Technical University of Denmark, Lyngby, Denmark, 1992.
- Munters W. & Meyers J. (2018). Optimal dynamic induction and yaw control of wind farms: effects of turbine spacing and layout. *Journal of Physics: Conference Series*, 0320125.
- Munters W., Meneveau C. & Meyers J. (2016). Turbulent inflow precursor method with time-varying direction for large-eddy simulations and applications to wind farms. *Boundary-layer Meteorology*, 305 – 328.
- Rampanelli G. & Zardi D. (2004). A Method to Determine the Capping Inversion of the Convective Boundary Layer. *Journal of Applied Meteorology* 43, 925 – 933.
- S.D. Downing and D.F. Socie. Simple rainflow counting algorithms. *International Journal of Fatigue*, 4(1):31 – 40, 1982.
- Sørensen, J. N. and Shen, W. Z.: Numerical modeling of wind turbine wakes, *Journal of fluids engineering*, 124, 393–399, 2002.
- Sørensen, N. N.: General purpose flow solver applied to flow over hills, Ph.D. thesis, Risø National Laboratory, Roskilde, Denmark, 1994.
- Townsend, A. A. R. (1976). *The Structure of Turbulent Shear Flow*. Cambridge University Press.
- Vitsas A. & Meyers J. (2016) Multiscale aeroelastic simulations of large wind farms in the atmospheric boundary layer. *Journal of Physics Conference Series*, 753:082020, 2016.
- Øye, S.: FLEX4 simulation of wind turbine dynamics, in: *Proceedings of the 28th IEA Meeting of Experts Concerning State of the Art of Aeroelastic Codes for Wind Turbine Calculations* (Available through International Energy Agency), 1996.